Indian Journal of Engineering & Materials Sciences
Vol. 30, August 2023, pp. 514-522
DOI: 10.56042/ijems.v30i4.4248

Microstructural, Thermal, and Adsorption Properties of Zeolitic Imidazolate Framework-8 Synthesized by a Facile Method

Roshini N[a], Nitin Prakash Lobo[b], Swarna V Kanth[a], & Sujata Mandal[a]*

[a]Centre for Human and Organizational Resources Development (CHORD), CSIR – Central Leather Research Institute, Chennai 600 020, India.

[b]Centre for Analysis, Testing, Evaluation & Reporting Services (CATERS), CSIR – Central Leather Research Institute, Chennai 600 020, India

Received: 21 July 2023; Accepted: 5 August 2023

The objective of the present research work is to green and facile synthesis of zeolitic imidazolate framework-8 (ZIF-8) metal-organic framework (MOF). Series of ZIF-8 (ZMOFs) have been synthesized by a facile mixing method with varying amounts of methanol as the reaction medium. The volume of methanol has been reduced up to 75% with respect to the required volume reported in the literature. All the synthesized ZMOFs show the crystallographic phase and chemical structure of zeolitic imidazolate framework-8 (ZIF-8) with reasonably high thermal stability. The specific surface area of the synthesized ZMOFs lies between 1185-1325 m^2g^{-1} and the pore volume between 0.51-0.56 cm^3g^{-1}. A decrease in the solvent volume results in a significant decrease in the product yield but has very little effect on the crystallinity, crystallographic phase, and pore characteristics of the synthesized ZMOFs.

Keywords: Metal-organic framework, Synthesis, Chemical characterization, Surface area, Porosity

1 Introduction

Zeolitic imidazolate framework-8 (ZIF-8) is a unique class of metal-organic frameworks (MOFs), which resemble a zeolitic (aluminosilicate) structural framework. In ZIF-8, the tetrahedrally coordinated transition metal ions (M = Zn, Fe, Co, Cu) are connected by an imidazolate (Im) bridge to form an M-Im-M network with a three-dimensional skeletal structure similar to zeolite.[1,2] ZIFs exhibit characteristics of both MOFs and zeolites, including similar crystallinity, porosity, and exceptional chemical and thermal stability. As a result, they combine the benefits of both types of materials.[3] ZIFs are found to be excellent adsorbent materials and have been used in both liquid and gas-phase adsorption applications.[1–4] ZIFs have also been used in drug delivery[5–7], photocatalysis[8,9], electrode materials for energy storage[10], and gas sensing[11,12] applications. Based on the desired application, the morphology, particle size, porosity, and surface functionality of ZIF-8 can be tuned by varying the synthesis methods, concentration, and composition of the precursor chemicals, synthesis medium, and reaction conditions.

In order to make the synthesis of ZIF-8 environmentally and economically sustainable, various green/solvent-free methods have been studied by many researchers.[13] Several methods such as solvothermal[14,15], sono chemical[16], microwave-assisted[17], mechanochemical, and microfluidic[18] have been used for the synthesis of ZIF-8 in various reaction mediums (solvent) like, DMF[18], methanol[14], water[19], acetone[20] and acetic acid[1]. Among all, methanol is the preferred reaction medium as it gets easily removed from the pores of ZIF-8 (less reactivity with ZIF-8), due to its small size and high volatility.[21] There are literature reports on the synthesis of ZIF-8 by varying the synthesis medium, precursor metal to ligand ratio [22], synthesis time, and temperature, and their effect on the microstructural properties of the synthesized ZIF-8. Venna et al. studied the growth of crystallization of ZIF-8 crystal as a function of synthesis time at room temperature and found that the average particle size and crystallinity increase with an increase of time.[23] Lai et al. have studied the synthesis of ZIF-8 nanoparticles at room temperature by varying synthesis time, the mole ratio of the precursor chemicals, and medium pH by microwave-assisted solvothermal method.[24] Lai et al. observed that ZIF-8 nanoparticles synthesized using higher concentrations of precursors have a higher crystallinity and larger particle size, while the specific surface area and the

*Corresponding author (E-mail: sujatamandal@rediffmail.com)

adsorption properties are not affected by the solvent volume.[24] Bustamante et al. have studied the impact of various solvents as reaction mediums on the physio-chemical properties of ZIF-8.[20]

The present research work aims for a facile synthesis of ZIF-8 using reduced volume of the reaction medium/solvent for their potential application as an adsorbent. The present study also aims to study the influence of reduced solvent volume on the microstructural, thermal, and adsorption properties of the ZIF-8. In the present research work, a series of zinc-based ZIF-8 (ZMOFs) have been synthesized by a facile mixing method and by varying the amount of reaction medium/solvent (methanol), keeping all other reaction parameters constant. The role of the volume of the reaction medium/solvent on the yield, morphology, crystallinity, particle size, surface area, porosity, and thermal stability of the ZMOFs has been investigated.

2 Materials and Methods

2.1 Materials

Zinc nitrate hexahydrate (AR grade) was procured from Sisco Research Laboratories Pvt. Ltd, 2-methylimidazole (2-MeIm) (97% purity) and methanol (99.9% purity) was procured from HiMedia laboratories, Pvt. Ltd., and ethanol (99.9% purity) was procured from BR Biochem Life Sciences Pvt. Ltd.

2.2 Synthesis of zinc-based ZIF-8 (ZMOF)

The ZMOF was synthesized by a modified method reported by Lee et al. [25] Bustamante et al. [20] and Zhang et al.[22] In this typical method, zinc nitrate hexahydrate (19 mmol) and 2-methylimidazole (158 mmol) were dissolved in 100 ml of methanol, and the solution was stirred in a magnetic stirrer at 25 °C and with 450 rpm speed for 24 hours. The white dispersion formed was then separated from the solvent using a centrifuge and the precipitate was washed thoroughly (three times) with ethanol. Then the precipitate was dried at 60 °C for 12 h in a hot air oven. The solid thus obtained was crushed into a fine powder and stored in a closed container. The MOF sample thus obtained was named ZMOF-1. The above procedure was repeated with 200 and 400 ml of methanol as solvent, keeping the same amount of zinc nitrate hexahydrate (19 mmol) and 2-methylimidazole (158 mmol) the same. The MOF samples obtained using 200 and 400 ml of methanol were named ZMOF-2 and ZMOF-4, respectively. A ratio of 1:8 was maintained between 2-MeIm and Zn in all the syntheses, based on the research report by Zhang et al.,[22] where 2-MeIm:Zn ratio of 8 was reported to give maximum yield with high crystallinity. The percentage yield of ZMOF was calculated following the method proposed by García-Palacín et al.[26], and the formula is presented in Equation 1.

$$Yield\ (\%) = \frac{ZMOF_{exp} - [ZMOF_{exp} - 8 \times \left(\frac{\%\,2-MeIm}{100}\right)]}{ZMOF_{th}} \times 100 \quad \ldots (1)$$

where $ZMOF_{exp}$ is the dry mass of ZMOF obtained after synthesis, the value of 2-MeIm percentage was obtained from the weight loss in TGA between 100 and 350 °C, $ZMOF_{th}$ is the theoretical yield considering the empirical formula of the theoretical synthesized ZMOF is $Zn(2\text{-}MeIm)_2$.

2.3 Characterization techniques

The crystallographic phase of the synthesized ZMOFs was studied by a Miniflex II Desktop X-ray diffractometer (XRD) from Rigaku Corporation, Japan. The XRD spectra were recorded in the 2θ range from 5 to 80 degrees using CuK_α radiation. The morphology and elemental composition were studied by Field Emission Scanning Electron Microscope (FE-SEM) and EDAX (TESCAN, CLARA, Czech Republic). The zeta potential and the hydrodynamic diameter were analyzed using the Zetasizer nano series, Malvern, United Kingdom. The surface area and porosity were analysed by the Brunauer-Emmett-Teller (BET) method and the data was collected using the BELLSORP instrument (Model Mini II) Japan. Prior to the surface area and porosity measurement, the samples were degassed at 200 ℃ for 3 hours. The Fourier Transform Infrared (FT-IR) spectra were recorded in a 4700 FT-IR spectrometer from Jasco, Japan. The Raman spectra were recorded in a LabRAM HR Evolution Confocal Raman Microscope from Horiba Scientific, France, using a 532 nm laser source. The thermal stability of the samples was analyzed in a temperature range from 25 to 800 ℃ (heating rate 20 ℃ per minute) under a nitrogen atmosphere using THEMYS one plus thermogravimetric analyzer (TGA) from Setaram Kep Technologies, France. The differential scanning calorimetry (DSC) data were collected in a temperature range from 25 to 350 ℃ (heating rate 10 ℃ per minute) under a nitrogen atmosphere using DSC 25 from TA Instruments, Canada.

The solid-state NMR experiments were performed on a Bruker Avance-III HD 400 WB NMR

spectrometer with ^{13}C, and ^{15}N resonance frequencies of 100.61, and 40.54 MHz, respectively. A double resonance 4 mm magic angle spinning (MAS) probe was used for the measurements, and all the samples were packed into 4-mm diameter zirconia rotors closed with Kel-F caps. The ^{13}C sideband-free spectrum was acquired using a cross-polarization total sideband suppression (CP-TOSS) scheme at a spinning speed of 5 kHz. The ^{13}C and ^{15}N chemical shifts were referenced externally to the glycine carbonyl signal at 176.03 ppm, and ^{15}N labeled NH_4Cl resonance at 39.3 ppm, respectively.

3 Results and Discussion

The percentage yield, zeta potential, and hydrodynamic diameter of the ZMOFs obtained with Zn:2-MeIm ratio 1:8 and by varying amounts of solvent (methanol) are presented in Table 1. The product yield increased with an increase in the solvent volume. There is a slight increase in the product yield on increasing the solvent volume from 100 to 200 ml however, on further increasing the solvent volume to 400 ml, the product yield increased by about two-fold. There is an increase in the zeta potential and a decrease in the hydrodynamic diameter of the ZMOFs on increasing the solvent volume.

The XRD spectra of the synthesized ZMOFs presented in Fig. 1 exhibit a similar diffraction pattern for all the samples. The diffraction peaks observed at 2θ positions 7.2°, 10.3°, 12.7°, 14.4°, 16.3°, 17.8°, 19.4°, 22.1°, 24.4°, 25.6°, 26.6°, and 29.6° correspond to the diffraction planes (011), (002), (112), (022), (013), (222), (123), (114), (223), (224), (015), and (044), respectively. The diffraction planes in Fig. 1 match well with those reported in the literature for the sodalite zeolitic imidazolate framework-8 (ZIF-8).[27] The ZMOF sample synthesized in minimum solvent (ZMOF-1) showed the highest peak intensity indicating the highest crystallinity among the three as-synthesized ZMOFs. The crystallinity of the ZMOFs follows the order ZMOF-1 > ZMOF-4 > ZMOF-2. The crystal sizes of ZMOF-1, ZMOF-2, and ZMOF-4 calculated using the Debye-Scherer equation are 42.27, 24.76, and 34.66 nm, respectively.[21] The crystal sizes of the ZMOFs are also in accordance with the sample's crystallinity. The XRD spectra presented in Fig. 1 signify that ZMOFs with high crystallinity can also be synthesized using a lesser volume of solvent than those reported in the literature.

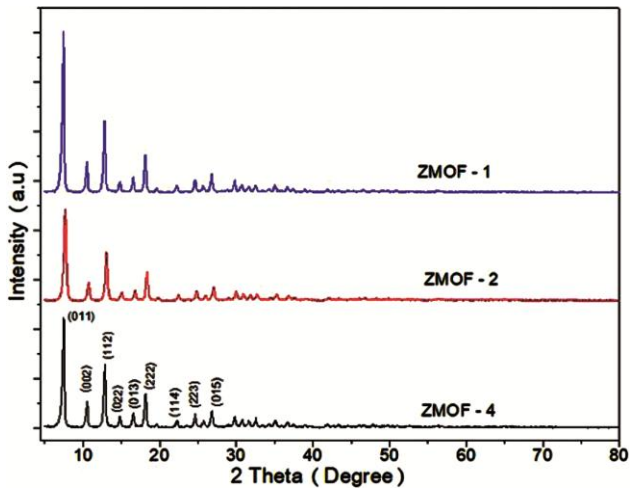

Fig. 1 — XRD patterns of the as-synthesized ZMOFs.

The FE-SEM micrographs of the as-synthesized ZMOF samples, recorded under two different magnifications are presented in Fig. 2. The synthesized ZMOF particles show a rhombic dodecahedron shape[27], which is probably the most stable morphology of ZIF-8.[3] The aggregated ZIF-8 particles are clearly visible in the FE-SEM images and the aggregation increased with an increase in the methanol volume. The maximum aggregation of ZIF-8 particles observed in ZMOF-4 might be due to its high yield. Moreover, the particle size also decreased with an increase in solvent volume.

The solubility of the precursor chemicals in the solvent (reaction medium) plays a significant role in the morphology and particle size of the ZMOF.[28] The nucleation process and crystal growth rate depend on the interaction and the reactivity of the precursor chemicals [$Zn(NO_3)_2$ and 2-MeIm] with the solvent. In the present case, both $Zn(NO_3)_2$ and 2-MeIm are highly soluble in methanol and hence generate Zn^{2+} ions and deprotonated 2-MeIm when dissolved in methanol. Therefore, when the volume of the methanol is less, the concentration of the precursor

Table 1 — The percentage yield, zeta potential, and hydrodynamic diameter of the synthesized ZMOFs

ZMOF Sample	Zn:2-MeIm ratio	Volume of solvent (ml)	Yield (%)	Zeta potential (mV)	Hydrodynamic diameter (nm)
ZMOF-1	1:8	100	24.4	-28.3	989.2
ZMOF-2	1:8	200	26.1	-20.9	770.2
ZMOF-4	1:8	400	47.1	-19.7	651.3

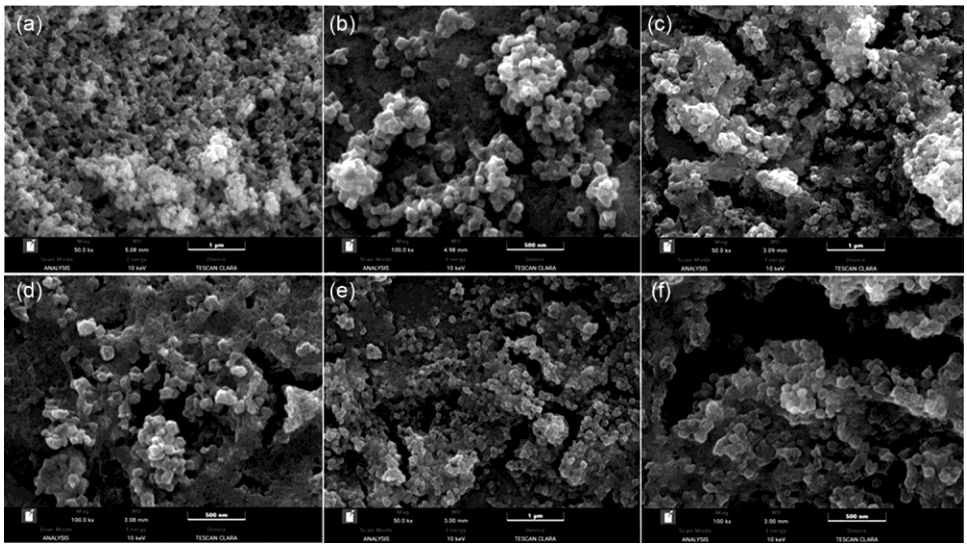

Fig. 2 — SEM micrographs of (a, b) ZMOF-1, (c, d) ZMOF-2, & (e, f) ZMOF-4.

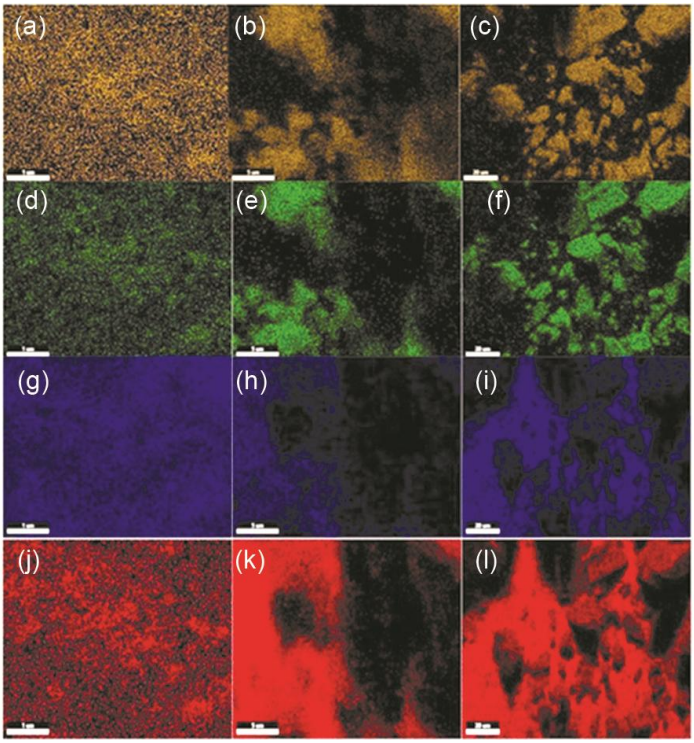

Fig. 3 — Elemental mapping of (a, d, g, j) ZMOF-1, (b, e, h, k) ZMOF-2, & (c, f, i, l) ZMOF-4 [Zinc: a, b, and c; Nitrogen: d, e, and f; Oxygen: g, h, and i; Carbon j, k, and l].

compounds is high, which reduces the formation of Zn^{2+} ions and the deprotonated 2-methyl imidazole in the methanol (reaction medium). Thus, due to ionization difficulty, the yield of the product is reduced with reduced solvent.[28] When the solvent volume is high, the concentration of the Zn^{2+} ion and the deprotonated 2-methyl imidazole is high. In the nucleation process, a large number of nuclei can only grow to smaller individual particles, which leads to a decrease in particle size. Therefore, the particle size of ZMOF-4 is less than that of ZMOF-1.

The elemental mappings of the ZMOF samples for Zn, N, C, and O are presented in Fig. 3 (a-l). In all the ZMOFs, the similar map pattern of zinc and nitrogen indicates that they are bonded together. Similarly, the exact map pattern of oxygen and carbon indicates

that the oxygen and carbon are in close vicinity or bonded together. Though the ZIF-8 structure also contains carbon, the major source of this carbon and oxygen might be CO_2, which further indicates the presence of trapped CO_2 within the ZIF-8 framework. Moreover, the aggregation of particles is clear in the mapping, and the aggregation increased with an increase in solvent volume following the order ZMOF-1 < ZMOF-2 < ZMOF-4.

Table 2 shows the specific surface area and pore volume of the synthesized ZMOFs obtained using the N_2 adsorption-desorption technique against those reported in the literature for ZIF-8 obtained by various methods, with varying Zn: 2-MeIm ratio and with various solvents. The variation in solvent volume has slightly affected the specific surface area of the ZMOFs. The specific surface area and pore volume of the ZMOFs increased with an increase in the solvent volume. ZMOF-4 shows the highest, and ZMOF-1 shows the lowest specific surface area and pore volume. Comparing the surface area and porosity values presented in Table 2 indicates that synthesis by solvothermal method yields ZIF-8 with a specific surface area between 1000 – 1500 m^2g^{-1} and total pore volume between 0.5-0.6 cm^3g^{-1} irrespective of the reaction conditions (time, temperature), except the one reported by Schjein et al. (2014) [29], which shows the exceptionally high surface area and higher pore volume of ZIF-8. The mixing method used in the present study yields ZIF-8 with a similar surface area and porosity as the solvothermal method. The microwave synthesis method yields ZIF-8 with low surface area and pore volume, compared to those synthesized by solvothermal or mixing methods (Table 2). Table 2 shows that the ZIF-8 obtained by the microemulsion method has a reasonably high surface area but exceptionally high pore volume.

The N_2 adsorption-desorption curves for all three ZMOF samples presented in Fig. 4a show a similar pattern, and the adsorption curve is typical of Type-I(a) isotherm, which indicates the microporous nature of the ZMOFs with narrow micropores of width ≤1 nm.[31] Among the three ZMOFs, ZMOF-4 showed maximum adsorption capacity. The BJH pore size distribution (Fig. 4b) shows that the ZMOFs are microporous in nature. In ZMOF-1 and ZMOF-4,

Table 2 — The specific surface area and pore volume of ZIF-8 were synthesized by various methods and under different reaction conditions

Synthesis Method	Solvent used	Zn: 2-MeIm ratio	Reaction Condition	Surface area (m^2g^{-1})	Pore volume (cm^3g^{-1})	Reference
Mixing method	MeOH	1:8	25°C, 24h			Present Study
ZMOF-1 (100 ml)				1185.2	0.51	
ZMOF-2 (200 ml)				1218.3	0.51	
ZMOF-4 (400 ml)				1324.9	0.57	
Solvothermal	MeOH	1:8	25°C, 1h	1700	0.66	29
Solvothermal	MeOH	1:1	25°C, 24h	1549	0.59	25
Solvothermal	DMF	1:1	140°C, 24h	1370	0.51	25
Solvothermal	DMF	1:2	120°C, 24h	1013	0.54	1
Solvothermal	Acetic acid	1:8	25°C, 24h	538	0.43	1
Microwave	*[bmim]BF_4	1:4	140°C, 1h	471	0.34	17
Micro-emulsion	heptane:hexanol (3:1)	1:2	25°C, 0.5h	1246	1.22	30

*[bmim]BF_4 -1-butyl-3-methyl-imidazolium tetra-fluoroborate

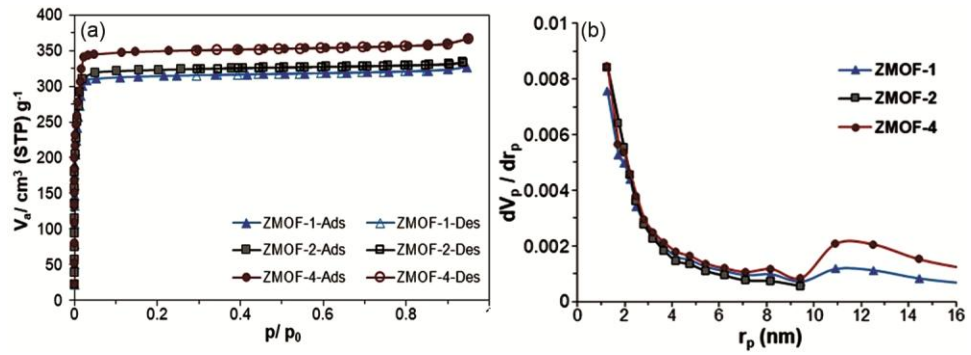

Fig. 4 — (a) Nitrogen adsorption-desorption, & (b BJH pore size distribution) curves of the synthesized ZMOFs.

there are very few pores above 10 nm, while ZMOF-2 has only micropores (Fig. 4b). The complete reversible adsorption is confirmed with the absence of hysteresis loop between the adsorption and desorption curves (Fig. 4a).[32]

The FT-IR spectra of the ZMOF samples are presented in Fig. 5a. All the synthesized ZMOF samples show the same spectral bands and match well with those reported in the literature for ZIF-8 structure.[33,34] The absorption bands characteristic of ZIF-8 structure are observed at 3133 cm^{-1} (C-H stretching, unsaturated hydrocarbon), 2928 cm^{-1} (C-H stretching, CH_3), 1628 cm^{-1} (C=C stretching), 1583 cm^{-1} (C=N stretching), 1370-1500 cm^{-1} (imidazole ring stretching), 1308 cm^{-1} (C-N stretching), 995 cm^{-1} (C-N bending), 756 cm^{-1} (C-H bending), and 422 cm^{-1} (Zn-N stretching).[1,22,27] Besides the characteristic ZIF-8 peaks, there is a distinct absorption peak at 2328 cm^{-1} attributed to the asymmetric stretching mode of CO_2.[34] The absorption bands at around 3600 and 3700 cm^{-1} (only in ZMOF-2) are due to the CO_2 combination modes. This indicates the adsorption of CO_2 from the atmosphere by the synthesized ZMOFs. All the synthesized ZMOF samples show the same spectral band frequencies with varying band intensity.

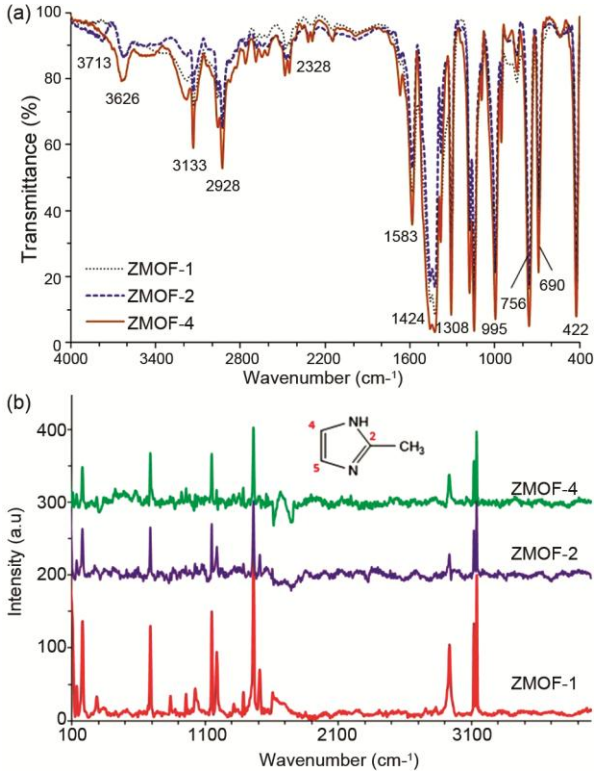

Fig. 5 — FT-IR spectra (a) and Raman spectra (b) of the synthesized ZMOFs.

Since the spectra were recorded by taking the same amount of sample, the band intensity can be considered as a quantitative representation of specific bonds. The intensity of all the bands is maximum for ZMOF-4 including those of CO_2. Therefore, the CO_2 adsorption by the ZMOFs can be considered in the order ZMOF-4 ≥ ZMOF-2 >>ZMOF-1.

The Raman spectra of the ZMOFs presented in Fig. 5b are similar but with varied peak intensities. The band observed at 182 cm^{-1} is assigned to Zn–N stretching, while the bands observed at 688 cm^{-1}, 1152 cm^{-1}, and 1463 cm^{-1} are attributed to out-of-plane bending vibration of the imidazole ring, C5–N stretching vibration, and methyl bending vibration, respectively.[35,36] The bands appearing at 1186 cm^{-1}, 1510 cm^{-1}, 2939 cm^{-1}, 3118 cm^{-1}, and 3140 cm^{-1} correspond to the C-N, C4-C5, C-H aromatic stretching vibrations respectively [37]. The antisymmetric stretching vibration of the C–H in the methyl group appears at 2939 cm^{-1}, and the C–H stretching vibration on the imidazole ring is observed at 3140 cm^{-1}.[35] These results further confirm the formation of the ZIF-8 structure in all the synthesized ZMOFs.

Figure 6 (a-b) depits the TGA and DTG thermograms of the synthesized ZMOFs. All the samples show around 3-4% weight loss up to 350 °C, which may be attributed to the removal of methanol, water, and/or CO_2 present in the cavities.[29] The weight loss between 100-350 °C is also due to the loss of extra-framework ligand (2-MeIm) if any.[26] All the samples remain stable up to 600 °C, and after 600 °C there is a sudden weight loss, which indicates the decomposition of the metal-organic bond of the ZIF-8 framework.[38] The weight loss between 600 – 800 °C was 22-23%. After 600 °C, the weight loss is due to the decomposition of the ZIF-8 wherein the organic ligands first get destroyed and finally the zinc oxide residue remains.[5,21,29] The percentage residue remained at 800 °C was 70.9, 72.2, and 73.6 for ZMOF-1, ZMOF-2, and ZMOF-4, respectively. The total weight loss recorded at 800 °C is much less than those reported in the literature[5,29] indicating high stability of the synthesized ZMOFs. However, a highly stable ZIF-8 similar to the present study has been reported by Yin et al.[39] Based on the TGA study, Yin et al. reported that the threshold temperature to maintain the ZIF-8 structure under an inert atmosphere is 500 °C, where the TGA experiment was performed with a heating rate of 5 °C /min. The

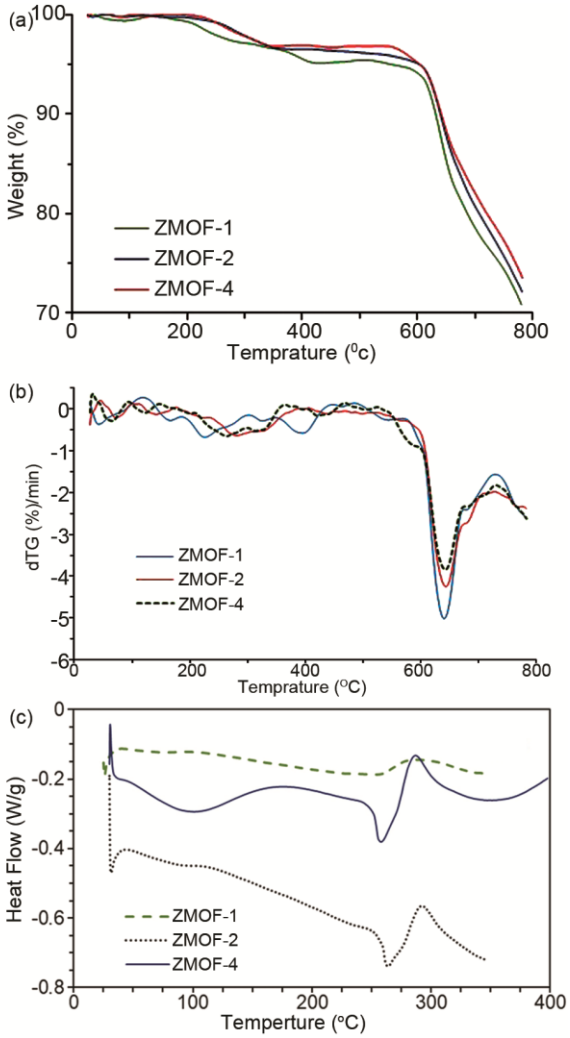

Fig. 6 — (a) TGA, (b) DTG, & (c) DSC thermograms of the ZMOFs.

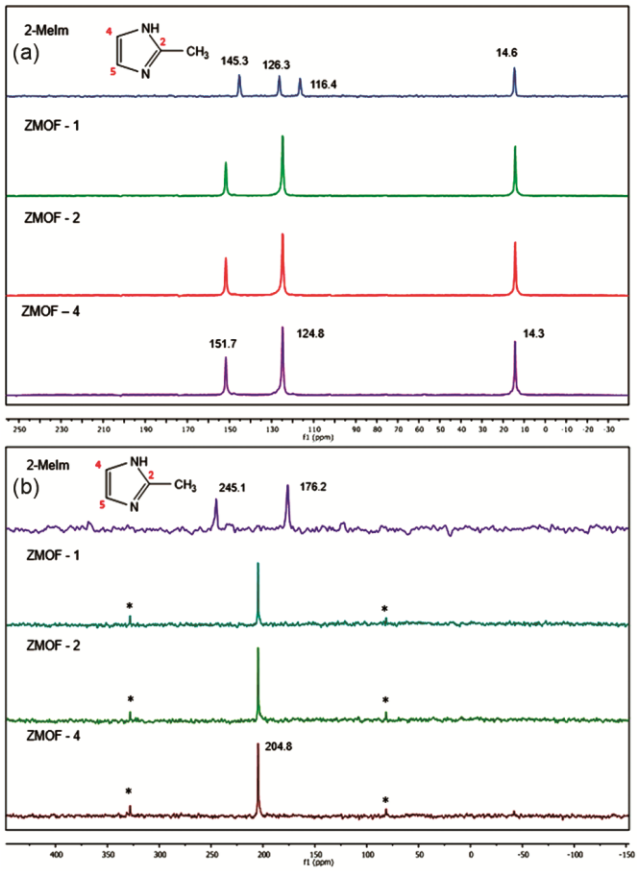

Fig. 7 — (a) ^{13}C CP-TOSS NMR spectra, & (b) ^{15}N CP-MAS NMR spectra of ZMOFs (*Spinning side bands).

difference in thermal stability of the synthesized ZMOFs in the present study and those reported by Yin et al. is primarily due to the difference in heating rate followed in the TGA experiment. [39]

The DSC thermograms of the samples are presented in Fig. 6c. All the ZMOFs show two endothermic peaks, the first peak below 150 °C and the second peak between 250-290 °C. The first endothermic peak is related to the evaporation of solvent/moisture, and the second endothermic peak is attributed to the desorption of physically adsorbed CO_2. [40] The intensity of the endothermic peak at around 262 °C in both ZMOF-2 and ZMOF-4 indicates a reasonably high amount of trapped CO_2 in the ZIF-8 framework. The presence of CO_2 is also evidenced in the EDAX mapping (Fig. 3) and in the FT-IR study (Fig. 5a) of the synthesized ZMOFs. In FT-IR spectra, the intensities of the absorption band corresponding to CO_2 were high for both ZMOF-2 and ZMOF-4 compared to those of ZMOF-1. Since ZIF-8 is a good adsorbent for CO_2 and the process is spontaneous, it is expected that CO_2 has been adsorbed from the atmosphere during the aging or post-synthesis processing (drying, grinding) of the ZMOFs.

The ^{13}C CP-TOSS NMR spectra of ZMOFs and 2-MeIm are presented in Fig. 7a of the samples. The ^{13}C NMR spectrum of 2-MeIm (2-methylimidazole) shows four distinct peaks at 145.3, 126.3, 116.4, and 14.6 ppm representing the four different carbon atoms present in the 2-methylimidazole ring. [41] All three ZMOF samples show three sharp peaks at 14.3, 124.8, and 151.7 ppm. The peak at 14.3 ppm is attributed to the methyl group attached to the imidazole ring, the peak at 124.8 ppm corresponds to the (N-CH=CH-N) C4 and C5 of the imidazole ring, and the peak at 151.7 ppm displays (N=C-CH_3-N) the C2 carbon. The appearance of sharp peaks suggests a relatively ordered structure for ZMOFs. [42] Morris et al. have also reported similar results for the ZIF-8 compounds

in the investigation of frameworks by nuclear magnetic resonance spectroscopy and single-crystal diffraction studies. [43] During the formation of the ZMOFs, the carbon in the fourth and fifth positions in 2-methylimidazole becomes chemically equivalent, so they appear as a single peak at 124.8 ppm in the ^{13}C NMR of ZMOFs. All the ZMOFs show a similar spectral profile, and the variation of peak intensities does not necessarily correspond to the population at different sites, since the obtained cross-polarised ^{13}C spectra are not quantitative. [41] In ZMOFs, all the resonating peaks of the organic linker atoms are found between 100 and 160 ppm, indicating the aromatic nature of the linker and the presence of the diamagnetic Zn metal center. [42]

The ^{15}N CP-MAS NMR spectra of the ZMOFs and 2-MeIm are presented in Fig. 7b. The ^{15}N NMR spectrum of 2-MeIm shows two peaks at 176.2 ppm (C4-NH-C2) and 245.1 ppm (C5-N=C2). The ^{15}N NMR spectra of all the ZMOFs show a single sharp resonance peak at 204.8 ppm.[43] The sharp peak results from the ordered structure of these materials. Further, the single peak's appearance in the ZMOFs indicates the chemical equivalence of the Nitrogen atoms, indicating that both the N atoms in the 2-methylimidazole ring are attached to the central Zn^{2+} atom. During the process of formation of ZMOF from 2-MeIm, the N-H group in the 2-methylimidazole gets deprotonated and forms a bond with the central Zn^{2+} atom in the ZMOF. The single peak in the NMR indicates that the deprotonated N atom of 2-MeIm bonds with the metal atom (Zn) and there is no other free 2-methylimidazole in the sample, confirming the purity of the synthesized ZMOF samples.

4 Conclusion

Zeolitic imidazolate framework-8 (ZMOF) ZIF-8, has been synthesized by a facile mixing method with varying amounts of reaction medium/solvent (methanol). The volume of solvent has been reduced up to 75% with respect to the volume reported in the literature. The microstructural, physicochemical, and thermal properties of the ZMOFs obtained by using standard and reduced volumes of solvent are compared. XRD studies confirm the zeolitic imidazolate framework-8 (ZIF-8) of all the synthesized ZMOFs. The purity of the ZIF-8 has been confirmed by FT-IR, Raman and ^{13}C, and ^{15}N solid-state NMR spectroscopy. The N_2 adsorption-desorption curves of all three ZMOF samples show Type-I(a) isotherm typical of microporous materials with narrow micropores of width ≤1 nm. The specific surface area and pore volume of the synthesized ZMOFs are reasonably high with surface area values between 1185-1325 m^2g^{-1} and pore volume between 0.51-0.56 cm^3g^{-1}. The ZMOFs are thermally stable up to 600 °C after which decomposition of the framework happens resulting in a sharp weight loss as shown in the TGA curve. The FT-IR and DSC studies show a reasonable amount of trapped CO_2 with the ZIF-8 framework of the ZMOF-4 and ZMOF-2, sample synthesized with in the standard volume and 50% reduced volume of methanol, respectively.

In conclusion, a decrease in the volume of the reaction medium/solvent (methanol) results in a significant decrease in the product yield but has very little effect on the crystallinity and crystallographic phase of the synthesized ZMOFs. The reduction in product yield with a decrease in the volume of the reaction medium is primarily due to the high concentration of the precursor chemicals in the reaction medium (methanol) leading to a decrease in the degree of ionization of the precursor chemicals and hence the product yield. Furthermore, a decrease in reaction medium also has a negative effect on the surface area and pore volume of the synthesized ZMOF and hence on their adsorption properties. Therefore, the study shows that synthesis of ZIF-8 in 75% reduced solvent volume is possible without a reasonable change in the microstructural, physicochemical and thermal characteristics, which can be a step towards the eco-friendly synthesis of ZIF-8.

Acknowledgement

Roshini acknowledged the project assistantship funding received from the project NWP0100. All the authors acknowledge the support received from CLRI-CATERS for all characterizations. CSIR-CLRI communication no. 1870.

References

1 Santoso E, Ediati R, Istiqomah Z, Sulistiono DO, Nugraha RE, Kusumawati Y, Bahruji H, Prasetyoko *Micropor Mesopor Mat*, 310 (2021).
2 Hassan N, Shahat A, Eldidamony A, Eldesouky MG, Bindary E, Mor A, Shahat A, El-Didamony A, El-Desouky MG, El-Bindary AA, *J Chem*, 8 (2020).
3 Bergaoui M, Khalfaoui M, Awadallah-F A & Al-Muhtaseb S, *J Nat Gas Eng*, 96 (2021).
4 Jabbari V, Veleta JM, Zarei-Chaleshtor M, Gardea-Torresdey J & Villagrán D, *Chem Eng J*, 304 (2016) 774.
5 Kaur H, Mohanta GC, Gupta V, Kukkar D & Tyagi S, *J Drug Deliv Sci Technol*, 41 (2017) 106.

6 Azizi Vahed T, Naimi-Jamal MR & Panahi L, *J Drug Deliv Sci Technol*, 49 (2019) 570.
7 Soltani B, Nabipour H & Nasab NA, *J Inorg Organomet Polym Mater*, 28 (2018) 1090.
8 Wang Z Lai C, Qin L Fu Y, He J Huang D, Li B Zhang M, Liu S Li L, Zhang W Yi H, Liu X, Zhou X, *Chem Eng J*, 392 (2020).
9 Huang S, Zhao J Wu C, Wang X Fei S, Zhang Q, Wang Q, Chen Z, Uvdal K, Hu Z, *Chem Eng Sci*, (2019) 209.
10 Siva V, Murugan A, Shameem A, Thangarasu S & Bahadur SA, *J Inorg Organomet Polym Mater*, 32 (2022) 4707.
11 Qin Y, Ding W & Zhao R, *Chem Phys Lett*, 781 (2021) 138965.
12 Zhan M, Hussain SA, Garni T, Shah S, Liu J, Zhang X, Ahmad A, Javed M, Qiao G, Liu G , *Mater Res Bull*, 136 (2021) 111133.
13 Gugin NY, Villajos JA, Dautain O, Maiwald M & Emmerling F, *ACS Sustain Chem Eng*, (2022)
14 Malekmohammadi M, Fatemi S, Razavian M & Nouralishahi A, *Solid State Sci*, 91 (2019) 108.
15 Saghir S & Xiao Z, *Mater Res Bull*, 141 (2021).
16 Bazzi L, Ayouch I, Tachallait H & EL Hankari S, *Results Eng*, 13 (2022).
17 Yang L & Lu H *Chin, J Chem*, 30 (2012) 1040.
18 Chen Y & Tang S, *J Solid State Chem*, 276 (2019) 68.
19 Jian M, Liu B, Zhang G, Liu R & Zhang X *Colloids Surf A, Physicochem Eng Asp*, 465 (2015) 67.
20 Bustamante EL, Fernández JL & Zamaro JM, *J Colloid Interface Sci*, 424 (2014) 37.
21 Akhundzadeh Tezerjani A, Halladj R & Askari S, *RSC Adv*, 11 (2021) 19914.
22 Zhang Y, Jia Y, Li M & Hou L, *Sci Rep*, 8 (2018).
23 Venna SR, Jasinski JB & Carreon MA, *J Am Chem Soc*, 132 (2010) 18030.
24 Lai LS, Yeong YF, Lau KK & Shariff AM in, *Procedia Eng*, 148 (2016) 35.
25 Lee YR, Jang MS, Cho HY, Kwon HJ, Kim S, Ahn WS, *Chem Eng J*, 271 (2015) 276
26 García-Palacín M, Martínez JI, Paseta L, Deacon A, Johnson T, Malankowska M, Téllez C, Coronas *ACS Sustain Chem Eng*, 8 (2020) 2973.
27 Wang Y, Zhao W, Qi Z, Zhang L, Zhang Y, Huang H, Peng Y, *Chem Eng J*, 394 (2020).
28 Chi WS, Hwang S, Lee SJ, Park S, Bae YS, Ryu DY, Kim JH, Kim J, *J Memb Sci*, 495 (2015) 479.
29 Schejn A, Balan L, Falk V, Aranda L, Medjahdi G, Schneider R, *CrystEngComm*, 16 (2014) 4493.
30 Zheng W,*Sep Purif Technol* , (2019) 111.
31 Thommes M, Kaneko K, Neimark AV, Olivier JP, Rodriguez-Reinoso F, Rouquerol J, Sing KS, *Pure Appl Chem*, 87 (2015) 1051.
32 Ghorbani H, Ghahramaninezhad M & Niknam Shahrak M, *J Solid State Chem*, 289 (2020).
33 Hu Y, Liu Z, Xu J, Huang Y & Song Y, *J Am Chem Soc*, 135, (2013) 9287.
34 Hu Y, Kazemian H, Rohani S, Huang Y & Song Y *Chem, Commun* , 47 (2011) 12694.
35 Li J, Chang H, Li Y, Li Q, Shen K, Yi H, Zhang, J *RSC Adv*, 10 (2020) 3380.
36 Cheng L, Yan P, Yang X, Zou H, Yang H, Liang H, *Mater Chem Phys*, 247 (2020).
37 Kolmykov O, Commenge JM, Alem H, Girot E, Mozet K, Medjahdi G, Schneider R, *Mater Des*, 122 (2017) 31.
38 Wang S & Zhang S, *J Inorg Organomet Polym Mater*, 27 (2017) 1317.
39 Yin H, Kim H, Choi J & Yip ACK, *Chem Eng J*, 278 (2015) 293.
40 Missaoui N, Kahri H & Demirci UB, *J Mater Sci*, 57 (2022) 16245.
41 Baxter EF, Bennett TD, Mellot-Draznieks C, Gervais C, Blanc F, Cheetham AK, *Phys Chem Chem Phys*, 17 (2015) 25191.
42 Sneddon S, Kahr J, Orsi AF, Price DJ, Dawson DM, Wright PA, Ashbrook SE *Solid State Nucl Magn Reason*, 87 (2017) 54.
43 Morris W, Stevens CJ, Taylor RE, Dybowski C, Yaghi OM, Garcia-Garibay MA *J Phys Chem C*, 116 (2012) 13307.